NASA/TM–20230018450

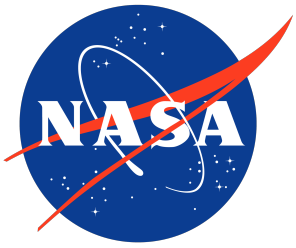

# Background Turbulence Characterization of the Curved Duct Test Rig

*Alexander N. Carr*
*Langley Research Center, Hampton, Virginia*

*Brian M. Howerton*
*Langley Research Center, Hampton, Virginia*

February 2024

# NASA STI Program Report Series

Since its founding, NASA has been dedicated to the advancement of aeronautics and space science. The NASA scientific and technical information (STI) program plays a key part in helping NASA maintain this important role.

The NASA STI program operates under the auspices of the Agency Chief Information Officer. It collects, organizes, provides for archiving, and disseminates NASA's STI. The NASA STI program provides access to the NTRS Registered and its public interface, the NASA Technical Reports Server, thus providing one of the largest collections of aeronautical and space science STI in the world. Results are published in both non-NASA channels and by NASA in the NASA STI Report Series, which includes the following report types:

- TECHNICAL PUBLICATION. Reports of completed research or a major significant phase of research that present the results of NASA Programs and include extensive data or theoretical analysis. Includes compilations of significant scientific and technical data and information deemed to be of continuing reference value. NASA counterpart of peer-reviewed formal professional papers but has less stringent limitations on manuscript length and extent of graphic presentations.

- TECHNICAL MEMORANDUM. Scientific and technical findings that are preliminary or of specialized interest, e.g., quick release reports, working papers, and bibliographies that contain minimal annotation. Does not contain extensive analysis.

- CONTRACTOR REPORT. Scientific and technical findings by NASA-sponsored contractors and grantees.

- CONFERENCE PUBLICATION. Collected papers from scientific and technical conferences, symposia, seminars, or other meetings sponsored or co-sponsored by NASA.

- SPECIAL PUBLICATION. Scientific, technical, or historical information from NASA programs, projects, and missions, often concerned with subjects having substantial public interest.

- TECHNICAL TRANSLATION. English-language translations of foreign scientific and technical material pertinent to NASA's mission.

Specialized services also include organizing and publishing research results, distributing specialized research announcements and feeds, providing information desk and personal search support, and enabling data exchange services.

For more information about the NASA STI program, see the following:

- Access the NASA STI program home page at http://www.sti.nasa.gov

- Help desk contact information:

https://www.sti.nasa.gov/sti-contact-form/
and select the "General" help request type.

NASA/TM–20230018450

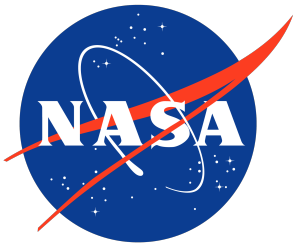

# Background Turbulence Characterization of the Curved Duct Test Rig

*Alexander N. Carr*
*Langley Research Center, Hampton, Virginia*

*Brian M. Howerton*
*Langley Research Center, Hampton, Virginia*

National Aeronautics and
Space Administration

Langley Research Center
Hampton, Virginia 23681-2199

February 2024

The use of trademarks or names of manufacturers in this report is for accurate reporting and does not constitute an official endorsement, either expressed or implied, of such products or manufacturers by the National Aeronautics and Space Administration.

Available from:

NASA STI Program / Mail Stop 050
NASA Langley Research Center
Hampton, VA 23681-2199

## Abstract

Interest in applying acoustic treatment to nontraditional locations of turbofan engines has led to recent testing of acoustically treated airfoils in the NASA Langley Curved Duct Test Rig. Current testing focuses only on sound attenuation by the sample when exposed to an incident sound field driven by a loudspeaker array. However, there may be much to gain from an aeroacoustic study of the interaction of turbulence with treated airfoils, especially in the case of acoustically treated outlet guide vane designs. Thus, the intent of this study is to take the first step in assessing the aeroacoustic quality of the NASA Langley Curved Duct Test Rig (typically only used for grazing flow studies) by examining the flow quality. The background turbulence levels are measured using hot-wire anemometry just upstream of the test section. Measurements indicate that the turbulence intensity is less than 0.3% in the core region of the flow. The autospectral densities show cavity tones and weak vortex shedding present in the core. The vortex shedding is determined to be from the upstream total pressure probe used to determine flow speed. The cavity tones are found to be the fundamental and harmonic frequencies of a porous ceramic tubular acoustic liner sample that separates the acoustic drivers from the flow region. Recommendations for improving the aeroacoustic quality of the tunnel are provided, such as removing the upstream probe and redesigning the ceramic tubular liner. Future acoustic characterization of the background levels is also recommended to further understand the feasibility of aeroacoustic studies in CDTR.


## Nomenclature and Abbreviations

| | | |
|---|---|---|
| CDTR | = | Curved Duct Test Rig |
| CTA | = | Constant Temperature Anemometry |
| $\overline{e}$ | = | Average voltage |
| $f$ | = | Frequency |
| $f_s$ | = | Sampling frequency |
| GFIT | = | Grazing Flow Impedance Tube |
| $\mathrm{I}\phi_1'$ | = | Streamwise turbulence intensity |
| LTF | = | Liner Technology Facility |
| $M$ | = | Mach number |
| $NWTC$ | = | National Wind Tunnel Complex |
| PTFE | = | Polytetrafluoroethylene |
| $R_{11}$ | = | Time autocovariance of the streamwise fluctuating mass flux |
| $\mathrm{Re}_h$ | = | Hydraulic Reynolds number |
| $S_{11}$ | = | Autospectral density of the streamwise fluctuating mass flux |
| St | = | Strouhal number |
| $t$ | = | Time |
| $T$ | = | Period of signal |
| $u_i$ | = | Flow velocity, where $i \in \{1, 2, 3\}$ denotes component of vector |
| $u_i'$ | = | Fluctuating component of velocity |
| $\overline{u}_i$ | = | Time average value of velocity |

| | | |
|---|---|---|
| $\rho$ | = | Density |
| $\rho_i'$ | = | Fluctuating component of density |
| $\overline{\rho}_i$ | = | Time average value of density |
| $\phi_i$ | = | Mass flux, $\rho u_i$ |
| $\phi_i'$ | = | Fluctuating component of mass flux |
| $\overline{\phi}_i$ | = | Time average value of mass flux |
| $\langle\rangle$ | = | Ensemble average of a quantity |

# 1 Introduction

Increased demand for aircraft noise reduction from regulators and industry alike, coupled with new open-rotor engine designs, have led to interest in acoustic treatment in nontraditional locations such as the engine bifurcation and outlet guide vanes. Acoustic liners are traditionally installed in the interior walls of the engine nacelle. Thus, analysis of new liner designs early in the development cycle often involves placing a liner sample in the sidewall of a grazing flow rig, exposing it to incident sound, and measuring attenuation or educing the impedance of the sample. The NASA Langley Liner Technology Facility (LTF) contains two grazing flow test rigs that are well suited to perform this type of analysis, the Grazing Flow Impedance Tube (GFIT) and the Curved Duct Test Rig (CDTR). Future tests may focus on treated bifurcations and outlet guide vanes. However, only the CDTR has a test section large enough to handle a treated bifurcation or outlet guide vane design, and thus, the GFIT may not be considered for these types of tests.

Testing treated engine bifurcation and outlet guide vane designs in the LTF introduces a new set of challenges caused by the placement of test articles in the flow. Blockage from the test article will reduce the overall achievable Mach number, and the flow downstream of the test section will be altered by its wake. This wake may affect how acoustic processing of data from the in-duct microphone array downstream of the test section is performed. Perhaps the most undesirable challenge for future aeroacoustic testing, however, would be the introduction of tonal or broadband sound from the interaction of the test article with any existing background turbulence in the duct. Thus, the objective of this study is to quantify background turbulence levels in CDTR with hot-wire anemometry measurements in order to make a preliminary assessment of the aeroacoustic and flow quality of the test rig. Special attention is given to the identification of coherent sources of fluid motion, as this type of motion may produce audible tones that would likely need to be reduced for future studies.

Although traditional experimental techniques of acoustic liner analysis focus on attenuation of sound introduced into the duct via acoustic drivers, there is much to gain from an aeroacoustic analysis of turbulence-airfoil interaction with acoustically treated airfoils. This is especially true for outlet guide vanes since their interaction with the rotor wake is primarily responsible for the generation of fan tones in turbofan engines [1]. Studies of turbulence-airfoil interaction have been performed in the past in aeroacoustic wind tunnels with low background noise levels [2–5]. In the LTF, the CDTR is capable of testing treated airfoil designs, as Nark and

Jones [6] have shown in their investigation of attenuation from a treated bifurcation design. However, the CDTR was not designed as an aeroacoustic wind tunnel with low background noise levels, and questions remain regarding the feasibility of an aeroacoustic study in this facility. Perhaps the two most important questions are as follows: (1) will tones produced by turbulence-airfoil interaction appear in acquired microphone data above the background levels, or could they be extracted from the background levels, and (2) will tones appear from the interaction of turbulence generated by other duct components with the airfoil? Hot-wire measurements obtained in the CDTR just in front of the test section will attempt to provide some insight into the answer to the second question.

Conventional wind tunnels generally have either a closed test section, or an open-jet test section [7]. From an aeroacoustic perspective, open-jet test sections benefit from low background noise levels due to the ability to put the test section in an anechoic environment. Additionally, microphones may be placed outside the jet, and thus avoid pressure fluctuations in the shear layer. In a closed test section, microphones are flush mounted to the duct walls and may be influenced by pressure fluctuations in the wall boundary layer. Aerodynamically, closed test sections realign the flow around an airfoil quickly, allowing for less correction required for blockage effects [7]. This is beneficial for source localization, as the acoustic emission is generated by sources in a flow that is more aerodynamically representative of an airfoil in a freestream that extends out in space infinitely [8].

A recent investigation of phased array measurements performed in a hybrid closed/open test section show that the closed test section measurements are contaminated from background noise and reflections, while the open test section measurements suffered from blurring from the decorrelation of acoustic waves passing through the shear layer [9]. However, Bahr [9] was able to show that accounting for image sources improves the closed test section noise source maps, while a coherence correction technique was able to mitigate blurring in the open-jet results. No noticeable change in the narrowband spectra of the closed test section results with or without the image source correction was observed, indicating that the image source correction only has an impact on source location identification. Further suggestions for improvement of closed test section measurements were suggested, such as applying background subtraction and correcting for the protective covering of the array. Acoustic measurements have also been performed in a Kevlar-lined foam-backed closed test section by Devenport et al. [10]. The Kevlar-lined test section provides the aerodynamic benefits of a closed test section with the ability to measure the acoustics with a microphone array that is outside the flow in an anechoic environment. One drawback, however, is the need to correct for sound attenuation through the boundary layer and Kevlar lining at different flow speeds. Devenport et al. [10] found up to 5 dB of attenuation for a flow speed of 72 m/s at 4 kHz and above.

The top achievable flow speed of many aeroacoustic tunnels reported in the literature appears to be below the $M = 0.5$ attainable in the CDTR, where $M$ is the Mach number, which may make it an attractive testbed for preliminary designs of acoustically treated airfoils. The higher flow speeds, however, result in higher background noise levels, which may limit the ability to obtain reliable acoustic spectra across the entire Mach number range without some background subtraction

technique. Although this is a concern, it may still be feasible to extract tonal sound information. Tonal information is generally more desirable than broadband information for the purposes of testing acoustic treatment, as the treatment is often designed to mitigate or attenuate the tonal noise components. As for determining source location, one possibility would be to use the approach of Bowen et al. [5] in their recent study of turbulence-airfoil interaction noise. They examined the coherence between microphone measurements and unsteady pressure measurements along the chord of an airfoil.

Clearly, background noise levels in a closed test section will play an important role in the feasibility of performing aeroacoustic measurements. In Lighthill's acoustic analogy [11], the source term for aerodynamic sound generated at small Mach number may be approximated as

$$\overline{\rho}\frac{\partial^2 u_i' u_j'}{\partial x_i \partial x_j}, \tag{1}$$

where $\overline{\rho}$ is the density of the medium and $u_i'$ are the fluctuating velocities. An immediate observation from this formulation is that the broadband background flow noise in the incompressible regime is largely influenced by the volume and levels of fluctuating Reynolds stresses present in the duct. Thus, the aeroacoustic quality of a wind tunnel may be inferred from direct measurement of $u_i' u_j'$. Additionally, aeroacoustic studies performed in any facility may benefit from direct measurement of $u_i' u_j'$, especially if a turbulence grid or shedding object is used to generate turbulence to which an airfoil or test apparatus is exposed.

Single-wire hot-wire measurements of the streamwise velocity, or mass flux in compressible flow, provide an estimate of the streamwise component of the fluctuating Reynolds stress. Pascioni et al. [8] state that turbulence intensities of less than 0.1% are desired, so that the critical Reynolds number for transition is not significantly affected, as demonstrated by Schlicting [12] for a flat plate boundary layer. The National Wind Tunnel Complex (NWTC) [13] recommends turbulence intensity of $\leq 0.7\%$. In the core of a closed test section, this is achievable; however, turbulence fluctuations in the fully developed boundary layer (or shear layer of an open jet) will certainly be higher than this. Model installation should thus attempt to avoid the boundary or shear layer.

In this study, single-wire hot-wire measurements are performed in the cross section of the CDTR just upstream of the test section to obtain the fluctuating mass flux. Section 2 outlines the experimental setup and data processing performed. Section 3 provides measured turbulence intensities and autospectral densities at various locations along the cross section, as well as some identification of coherent turbulence and acoustic tones and their potential sources. Finally, Sec. 4 states conclusions of the study.

# 2 Experimental Setup

## 2.1 Facility and Instrumentation

The CDTR is an open-loop wind tunnel that draws in atmospheric unconditioned air with a centrifugal fan. Currently, flow speeds up to $M = 0.5$ may be achieved in the CDTR. During testing, the maximum hydraulic Reynolds number ($\mathrm{Re}_h$) achieved, corresponding to $M = 0.5$, was approximately $2.2 \times 10^6$. The test section is a rectangular duct of 15.24 cm $\times$ 38.10 cm (6 in $\times$ 15 in). It was designed to assess the acoustic and aerodynamic performance of acoustic liner test samples, and the test section ranges between 100% and 25% of the scale of the engine aft-duct of a business jet or large commercial passenger aircraft, respectively. Sound may be generated using a 32 loudspeaker array, which may be placed either upstream (aft mode) or downstream of the test section (inlet mode). Fan noise from the centrifugal fan is mitigated with a Helmholtz resonator section downstream of the test section, but upstream of the fan. Figure 1 shows an illustration of the CDTR.

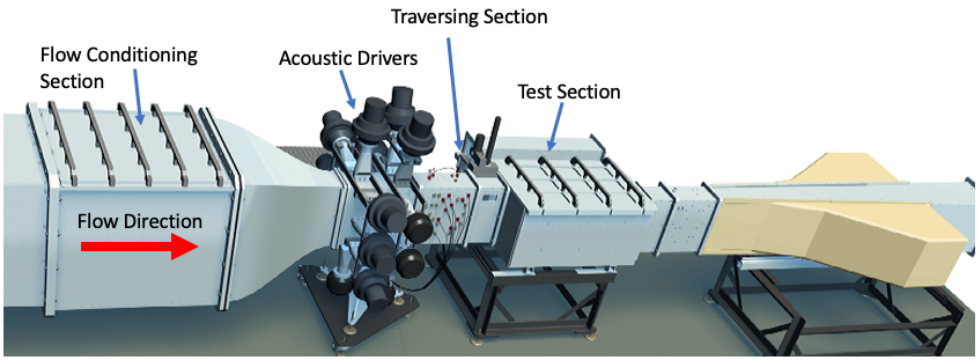


Figure 1: Artist rendering of CDTR.

Upstream of the test section, in the driver array section, there is a total pressure probe that sticks out from the center of the top of the duct into the core region. The total pressure measured from this probe, along with the static pressure tap at the test section entrance and a previous tunnel speed calibration are used to determine flow speed. Turning vanes are present in the bend just after the inlet section, to help prevent any large-scale vorticity formation. The flow conditioning section is present downstream of the turning vanes and upstream of the driver section and test section. It consists of three turbulence screens to reduce axial turbulence, along with a 3.81 cm-thick section of 0.48 cm hexagonal-cell aluminum honeycomb to break up lateral turbulence. These components are arranged with one screen at the entrance to the flow conditioning section, followed by the honeycomb 3.4 cm downstream. The two remaining screens are placed 39.2 and 79.84 cm downstream of the honeycomb, respectively. The screens are made from 1.57 mm stainless steel wire woven to eight mesh lengths per inch

The acoustic drivers are connected to the duct via transition sections that vary from a circular entrance cross section of 5.08 cm diameter to a rectangle 1.91 by 7.98 cm. In order to prevent tones from the transition cavities, a ceramic tubular

acoustic liner material was placed in the duct openings connected to each driver transition, flush with the duct inner surface. This material is called CT65, as it has an open area ratio of 65%. The material allows acoustic transmission while preventing flow entrainment into the transitions. The depth of the material is 1.27 cm (0.5 in) to match the thickness of the duct walls.

Constant temperature anemometry (CTA) is performed with a hot-wire probe. The probe has a 5 $\mu$m diameter, 1.25 mm-long platinum-plated tungsten wire sensor aligned normal to the flow direction. The hot-wire probe is connected to a CTA module operating in a 1:1 bridge mode. The control arm has a variable resistor to set desired overheat ratios of the anemometer. The overheat ratio was set to 0.828, such that the heated resistance of the sensing element was 1.828 times greater than its resistance at 20 °C. Multiple wires were employed throughout the test due to frequent wire breakage that will be discussed further in Sec. 2.2. The frequency response of each wire was estimated with a square-wave test at $M = 0.5$ in the center of the duct. The frequency response was generally observed to be $\geq 120$ kHz, which enabled sampling of the wire at frequencies high enough to capture most of the inertial range of the turbulence spectrum at the Reynolds numbers experienced here.

Along the duct cross section, 130 different locations were surveyed corresponding to a range of $0.762 \leq x \leq 13.36$ cm and $0.762 \leq y \leq 37.34$ cm ($0.3 \leq x \leq 5.258$ in and $0.3 \leq y \leq 14.7$ in), as shown in Fig. 2. Fewer measurements were performed in the core region, since the flow velocity is nearly constant in the core and turbulence levels are low. Also, measurements are performed closer to the $x = 0$ wall than to the $x = 15.24$ cm wall since the probe configuration made it difficult to reach the wall at $x = 15.24$. The hot-wire was sampled at 102.4 kHz. A total of 2,048,000 samples are taken at each measurement location, corresponding to 20 seconds of data in real time. The sampled signal was then split into a DC-coupled signal and an AC-coupled signal. A low-pass filter with cutoff at 30 Hz was applied to the DC signal to obtain average quantities. The AC signal was passed through a 4-pole Butterworth low-pass filter at 40 kHz three times to remove aliased components from the computed spectral density. In the post-processing stage, the AC signal is used to compute turbulence statistics by breaking up the signal into 2048 blocks of 1000 data points each.

## 2.2 Hot-Wire Breakage

During testing, hot-wire probes broke quickly and often, sometimes before calibration was even finished. Generally, hot-wire breakage could be caused by prong vibration, particulates in the duct impacting the wire, and overheating the wire. The flow speeds in this experiment are likely too low to cause prong vibration, and the overheat ratio of 0.828 is fairly standard. Thus, a test was performed to examine if particulates are present in the duct. A polytetrafluoroethylene (PTFE) plug was placed in the center of the duct at approximately the same location as the hot-wire during calibration. Then, the flow was increased to $M = 0.5$ and maintained for 15 minutes. After the test, the PTFE plug was examined for particulates. Figure 3 shows that many particulates were present on the plug after the test was per-

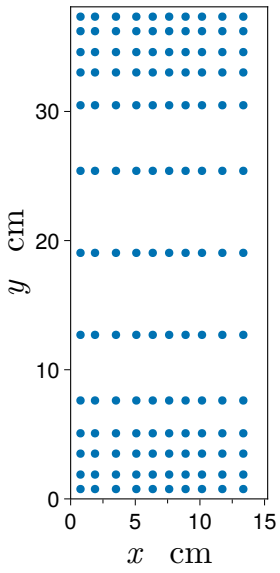


Figure 2: Measurement locations along cross section.

formed, leading to the conclusion that particulate impact of the wire was causing wire breakage.

Microscopic inspection of the PTFE plug revealed that the particulates are either brown or silver/gray in color. This indicates two likely causes of particulates in the flow. The first is that the CDTR intakes air from outside, and no particulate filter is present on the air intake. The brown particulates are likely brought in from the outside environment. The second is that oxidation of the aluminum duct walls has led to pitting, causing small flecks of aluminum to come off at high Mach numbers. The silver particulates are from the duct walls. The size of the particulates were estimated to range from 10 to 200 $\mu$m. Action will be taken in the future to reduce the number of particulates present in the flow by placing a particulate filter in the intake and treating the ductwork to resist further oxidation.

## 2.3 Hot-Wire Calibration

The hot-wire was calibrated in-duct by placing the probe on the centerline and relating the measured mean values of mass flux to the tunnel mass flux operating condition. The tunnel Mach number at the hot-wire traverse station is obtained from a tunnel calibration, performed by relating the measured total and static pressure at an upstream location to the measured total and static pressure from a Pitot-probe at the centerline of the hot-wire traversing station. Total temperature is measured upstream of the contraction of the duct, and the relative humidity is measured downstream of the test section in the resonator section. These quantities are used to back out Mach number and mass flux, so that during normal operation the upstream Pitot-static probe may be used in conjunction with the tunnel calibration data to estimate the mass flux at the hot-wire calibration location.

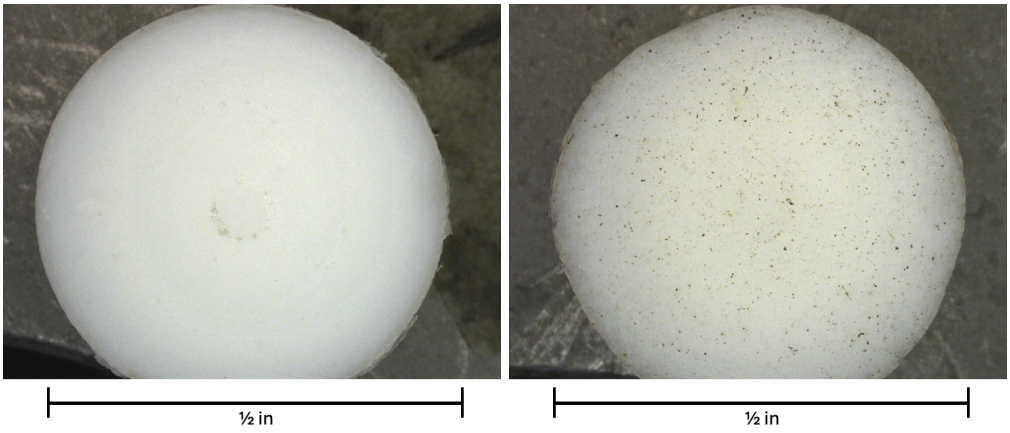


(a) (b)

Figure 3: PTFE plug surface (a) before and (b) after testing.

King et al. [14] showed that hot-wire response in the range $0.2 \leq M \leq 0.5$ is predominantly sensitive to mass flux, but also depends slightly on the Mach number. Since there is no way to control the mass flux and Mach number independently in the CDTR, one calibration of wire voltage to mass flux performed from $M = 0$ to 0.5 is adequate. Calibration of each wire was performed just before testing, in an effort to mitigate issues arising from changing environmental factors and the dual dependence on mass flux and Mach number. Slight inaccuracies arising from changing environmental factors were considered to be admissible for this initial study, since the main objective is to characterize the background turbulence levels of the CDTR and not necessarily to obtain precise mean flow measurements.

Let the mass flux be denoted $\phi_i = \rho u_i$. The streamwise average mass flux, $\overline{\phi_1}$ is assumed to be a polynomial function of the average voltage of the hot-wire, $\overline{e}$,

$$\overline{\phi_1} = \sum_{n=0}^{N-1} a_n \overline{e}^n. \tag{2}$$

The value of $N$ is set to 6 to compute a fifth-order polynomial, and 15 measurements of the hot-wire voltage are obtained across the operating range of the CDTR. The problem of determining the coefficients may be solved by a linear least-squares regression analysis. Once the coefficients are determined, the hot-wire data may be reduced to streamwise mass flux.

## 2.4 Data Processing

In the proceeding analysis, stationary flow is assumed, such that statistics computed from the time histories of $\phi_i$ at a single setpoint are independent of the choice of time origin. The data is post-processed by taking 1000 blocks of 2048 points each and performing ensemble averaging to find the mass flux covariance and autospectral density. Statistics such as the mean and variance are determined using a combination

of time averaging and ensemble averaging. An overbar denotes time averaging

$$\overline{\phi_i} = \frac{1}{T}\int_0^T \phi_i \mathrm{d}t, \tag{3}$$

or taking the average of some quantity over all frequencies, in the case of a variable in frequency space. Bracket notation denotes ensemble averaging

$$\langle \phi_i \rangle = \frac{1}{M}\sum_{m=1}^{M} \phi_i^{(m)}, \tag{4}$$

where $M$ is the number of realizations and a superscript in parentheses, $\phi_i^{(m)}$, denotes the $m^{\text{th}}$ realization of the mass flux. The fluctuating mass flux for a given realization is determined by subtracting the time average, $\phi_i' = \phi_i - \overline{\phi_i}$.

The mean fluctuating streamwise mass flux is $\langle \overline{\phi_1'} \rangle$, which should be interpreted as the ensemble average of the time average of each fluctuating streamwise mass flux realization. The variance is $\langle \overline{(\phi_1')^2} \rangle$. The streamwise turbulence intensity is defined as

$$\mathrm{I}\phi_1' = \frac{\sqrt{\langle \overline{(\phi_1')^2} \rangle}}{\langle \overline{\phi_1} \rangle}. \tag{5}$$

The time autocovariance of the streamwise fluctuating mass flux is

$$R_{11}(\tau) = \langle \overline{\phi_1'(t)\,\phi_1'(t+\tau)} \rangle, \tag{6}$$

and the autospectral density of the signal is the Fourier transform of the time autocovariance,

$$S_{11}(f) = \int_{-\infty}^{\infty} R_{11}(\tau)\, e^{-i2\pi f\tau} \mathrm{d}\tau. \tag{7}$$

The autospectral density is computed by

$$S_{11}(f) = \frac{1}{M}\sum_{m=1}^{M} \frac{1}{Nf_s} \left( \sum_{k=1}^{K} \phi_1'^{(m)}(t_k)\, e^{-i2\pi f t_k} \right) \left( \sum_{j=1}^{J} \phi_1'^{(m)}(t_j')\, e^{i2\pi f t_j'} \right), \tag{8}$$

for real-valued $\phi_1'$, where $M$ is the number of blocks, $N$ is the number of points per block, and $f_s$ is the sampling frequency. The two summations on the right-hand side may be computed using a fast Fourier transform.

# 3 Results

In Fig. 4, contour plots of turbulence intensity along the cross section of the duct are shown for $M = 0.1$ (Fig. 4a) and $M = 0.5$ (Fig. 4b). As mentioned in Sec. 2, measurements were made from 0.762 cm to 13.36 cm along the $x$ direction. In Fig. 4, the turbulence intensity beyond $x = 13.36$ cm, to $x = 14.48$ cm, is extrapolated assuming that the intensity at $x = 14.48$ cm matches the measurements at $x = 0.762$ cm. This was deemed a fair assumption after examination of turbulence intensity

profiles along the $y$ direction at various wall standoff distances in $x$, where a strong symmetry was observed around $x = 7.62$ cm. The turbulence intensity profiles at both $M = 0.1$ and $M = 0.5$ are very similar, with core regions in the range of $3 \leq x \leq 12$ cm and $8 \leq y \leq 30$ cm, roughly. Although it appears as if the core region could extend further out in $y$, for instance from 5 cm to 33 cm, there is a slight increase in turbulence intensity in the ranges $5 \leq y \leq 8$ cm and $30 \leq y \leq 33$ cm. This increase is due to contraction-induced crossflow that locally thickens the boundary layer along the wall centerline. A vortex pair can occur if the crossflow velocity component is large enough. The turbulence intensity increase caused by this crossflow is more pronounced as Mach number increases. Thus, to avoid this, it would be favorable to place any future test articles in the core region.

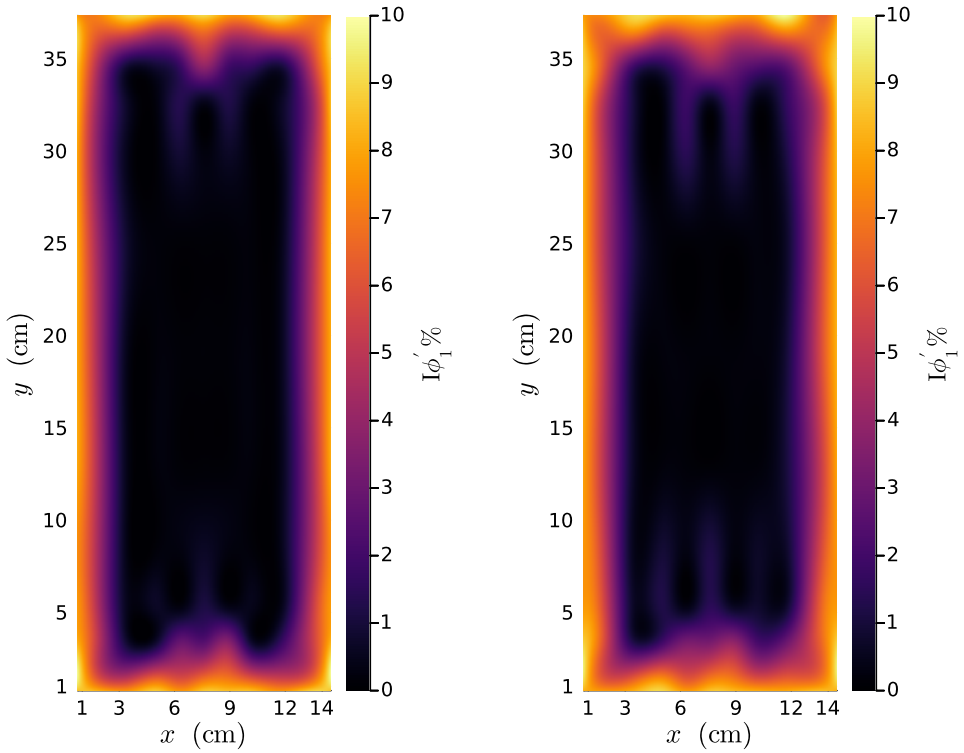


Figure 4: Contour plots of turbulence intensity for (a) $M = 0.1$ and (b) $M = 0.5$.

The turbulence intensity reaches maximum values of 9.77% and 9.78% in the boundary layer, and minimum values of 0.11% and 0.13% in the core region for $M = 0.1$ and $M = 0.5$, respectively. The turbulence intensity is nearly always below 0.3% in the core region for all Mach numbers. The spatial distribution of turbulence is fairly consistent across all Mach numbers, as indicated by Fig. 5. Figure 5 shows a contour plot of the absolute difference in turbulence intensity between $M = 0.1$ and $M = 0.3$ (Fig. 5a), and $M = 0.1$ and $M = 0.5$ (Fig. 5b). The maximum difference is on the order of 2%, and only occurs in the corner regions between the

0.1 and 0.5 cases. In the core region, the differences in turbulence intensity are almost negligible.

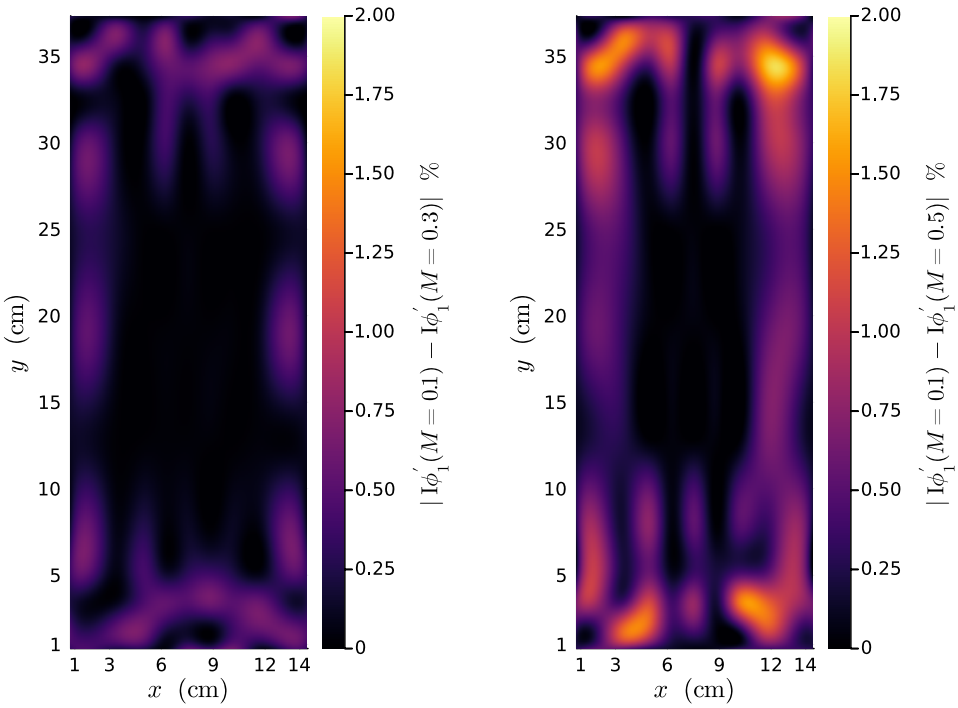


(a) (b)

Figure 5: Absolute difference in turbulence intensity between (a) $M = 0.1$ and 0.3, and (b) $M = 0.1$ and 0.5.

In Fig. 6, the autospectral densities at four different locations in the cross section are presented for all Mach numbers. In the core region, the turbulence intensity is low enough that the noise floor of the anemometer is encountered around 4 kHz for $M = 0.1$. This electrical noise appears as a rise in $S_{11}$ with a slope of $f^2$ at high frequencies. As the Mach number is increased, the frequency at which the noise floor of the anemometer is reached increases as well. The noise floor itself appears to increase in magnitude, indicating that $f^2$ noise increases in power as the voltage applied to the current increases. In the boundary layer regions, a $-5/3$ roll off in the inertial range of the spectrum is observed, which is to be expected. As the Mach number increases, the autospectral density increases in magnitude as well due to the increased turbulence fluctuation intensity.

At $x = 5.08$ cm and $y = 19.05$ cm, several spikes and humps in the autospectral densities across all five Mach numbers may be observed in Fig. 7. These spikes and humps correspond to sources of coherent fluid motion, which is undesirable when no test article is present in the duct and no sound is generated by the acoustic drivers. In Fig. 7, five tones appear at constant frequency across all Mach numbers with increasing amplitude as a function of the flow speed. This is characteristic of tones produced by standing waves present in open- or closed-ended tubes; the tones

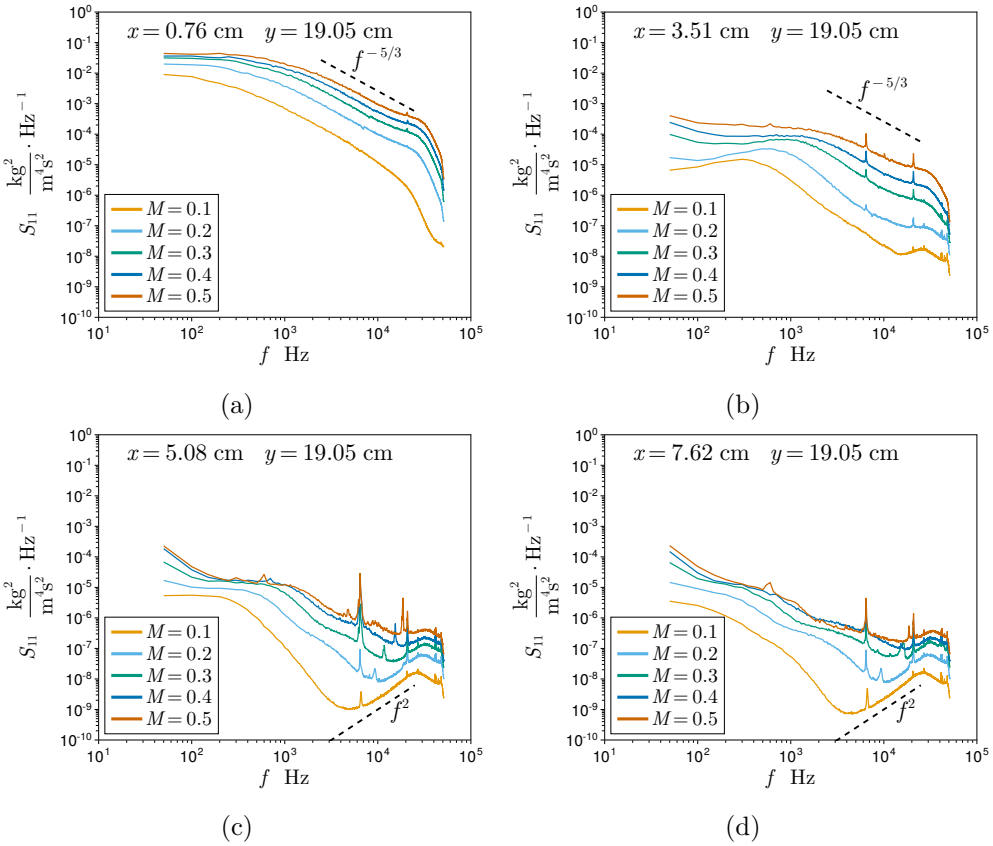


Figure 6: Autospectral densities of fluctuating mass flux at several $x$ locations with $y = 19.05$ cm: (a) $x = 0.76$ cm (boundary layer), (b) $x = 3.51$ cm (boundary layer), (c) $x = 5.08$ cm (core), and (d) $x = 7.62$ cm (core).

will be referred to here as cavity tones. The tone appearing at 6700 Hz is the first fundamental tone caused by the CT65 sample separating the driver transitions from the duct flow. The sample depth is 1.27 cm, corresponding to duct wall thickness, and acts like a quarter-wavelength resonator. Another tone appears at 20.75 kHz and corresponds to the third harmonic from the same quarter-wavelength resonator. The remaining $4^{\text{th}}$, $6^{\text{th}}$, and $7^{\text{th}}$ harmonics are present in Fig. 7 at higher frequencies, and dashed lines with the corresponding harmonic number are present to indicate where the harmonics are predicted to appear. These cavity tones should be mitigated before aeroacoustic testing takes place, as these tones even appear in autospectra of some of the boundary layer measurement data, which means that they might be strong enough to contaminate microphone data. Additionally, they are acoustic in nature, and any future turbulence generation mechanisms installed to alter the flow for turbulence-airfoil interaction studies would not change the presence of these tones. One such possible method for mitigating this would be to tape over the driver openings for any aeroacoustic testing. However, practically speaking, this would require the duct to be taken apart before and after each test, which is operationally undesirable.

A different coherent fluid motion, vortex shedding, appears in the shaded regions of Fig. 7 and is caused by the upstream total pressure probe. These shaded regions of Fig. 7 represent Strouhal (St) number ranges of 0.18 to 0.22, which is characteristic of vortex shedding from a cylinder in the Reynolds number range of interest (see [15]), for each Mach number. The vortex shedding hump in the spectrum is observed to increase in frequency as Mach number increases from 0.2 to 0.5 and falls within the appropriate Strouhal range for each flow speed, except for $M = 0.2$. The probe Reynolds number at $M = 0.2$ is 7493. Thus, according to the data in White [15], the Strouhal number will be at the high end of the 0.18 to 0.22 range. Some reasons that the vortex shedding frequency falls outside the predicted Strouhal number range at this flow speed may be due to uncertainty in the flow speed calculation, and possible 3D effects from the probe since the probe is installed at the top of the duct and only sticks out to about $y = 25.4$ cm. The vortex shedding is not present at $M = 0.1$, possibly because the probe is too far upstream and the vortices disperse at such a low Mach number before reaching the hot-wire measurement plane. This coherent turbulent motion is more localized to the upstream probe wake and much weaker in amplitude at the start of the test section as opposed to the cavity tones. Thus, it does not appear in boundary layer measurements, and would likely not be a significant factor in turbulence-airfoil interaction studies, as any turbulence generating mechanism placed upstream of the airfoil would likely contribute to further breakup of this weak coherent motion as well as generate its own stronger coherent (or incoherent) motion. Nevertheless, the upstream total pressure probe will be removed in the future in favor of static ports for detecting flow speed.

There is also coherent motion present in the $M = 0.5$ results at around 600 Hz and 5 kHz, as observed in Fig. 6. It is not yet clear what is causing these bumps in $S_{11}$ to appear; however, there are several possibilities. One possible cause of the 600 Hz bump is that the turning vanes upstream of the flow conditioning section are causing some coherent vortex motion at higher Mach numbers. A possible cause of

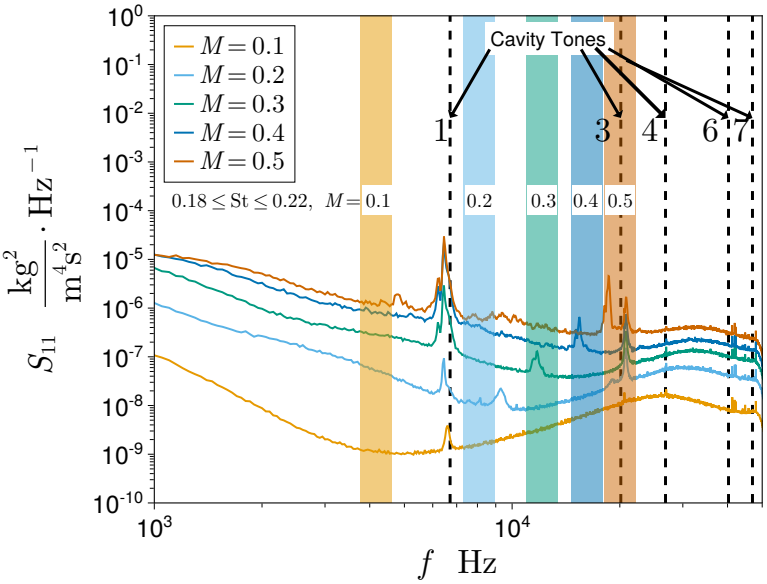


Figure 7: Zoomed in plot of autospectral densities at $x = 5.08$ cm and $y = 19.05$ cm. Predictions of upstream probe vortex shedding shown as shaded regions with color corresponding to Mach number. Cavity tone predictions shown as black dashed lines with labels corresponding to harmonic number.

the 5 kHz motion is vortex shedding from the total temperature probe upstream of the flow conditioning section. These two hypotheses are believed to be unlikely since the flow conditioning section should breakup such vortices. A more likely possibility for the bump at 5 kHz is vortex shedding from the hot-wire probe holder causing motion of the hot-wire itself at the measurement location. This is plausible since 5 kHz would correspond to vortex shedding of the 6.35 mm diameter probe holder at St $\approx 0.185$. For the 600 Hz bump, it could possibly be an acoustic disturbance caused by the turning vanes, but this must be investigated further. Inspection of microphone data in the future will help to determine whether that disturbance is acoustic or not, and whether it is coming from upstream or downstream of the test section.

## 4 Conclusions

In this study, hot-wire anemometry measurements performed in the cross section of the CDTR just upstream of the test section revealed coherent fluid motion present at several frequencies in the autospectral density plots. The spikes and humps in $S_{11}$ are consistent with a mixture of cavity tones and vortex shedding motion. The vortex shedding present from $M = 0.2$ to 0.5 aligns well with predictions of vortex shedding from the upstream total pressure probe. The cavity tones agree with predictions of the 1$^{\mathrm{st}}$, 3$^{\mathrm{rd}}$, 4$^{\mathrm{th}}$, 6$^{\mathrm{th}}$, and 7$^{\mathrm{th}}$ harmonics of the 1.27 cm CT65 samples separating the driver transitions from the flow. The 1$^{\mathrm{st}}$ and 3$^{\mathrm{rd}}$ harmonics are strong enough to contaminate boundary layer measurement data. Additionally, a 5 kHz

bump in the autospectrum at $M = 0.5$ likely corresponds to vortex shedding of the hot-wire probe holder, and the cause of a 600 Hz bump at the same Mach number is still unknown.

### 4.1 Recommendations for CDTR Capability Enhancement

Initial improvements to the aeroacoustic quality of the CDTR will focus on: (1) removing the upstream total pressure probe, and (2) modification of the material used to separate the driver transitions and flow, in order to reduce the cavity tones or push them to higher frequencies beyond the range of interest. The next step in the assessment of the CDTR to perform aeroacoustic testing is an acoustic background characterization. Measurements of the broadband flow noise currently measured by the flush-mounted microphones are required to determine the feasibility of making tonal or broadband measurements of turbulence-airfoil interaction. Additionally, the feasibility of an in-duct phased array for source mapping will also be considered, likely with background subtraction techniques in mind.

Future aerodynamic measurement capability, such as hot-wire anemometry, laser doppler velocimetry (LDV), or particle image velocimetry (PIV), may be desired to support testing of acoustically treated airfoils. Such capability enhancement would require modification to the CDTR. The first modification would involve duct treatment to prevent further aluminum oxidation, as well as a particulate filter on the intake. This would remove most of the particulates in the flow that are currently breaking hot-wires and would contaminate laser or particulate imaging measurement techniques. A second modification would be a test section modification to install a hot-wire traverse, or add viewing windows for LDV or PIV, in order to obtain measurements near the test article location. Installation of a hot-wire traverse would probably be more involved because adding viewing windows is likely made easier by the current liner sample drop-in procedure; a liner sample could be replaced by a viewing window. Of course, LDV and PIV require the additional step of seeding the flow, and further investigation is required to determine the feasibility of seeding in the CDTR.

## References


1. Tyler, J.M. and Sofrin, T.G., "Axial Flow Compressor Noise Studies," *SAE Transactions*, Vol. 70, 1962, pp. 309-332.

2. Moreau, S., Roger, M., and Jurdic, V., "Effect of Angle of Attack and Airfoil Shape on Turbulence-Interaction Noise," AIAA Paper 2005-2973, May 2004.

3. Hutcheson, F.V., Brooks, T.F., and Stead, D.J., "Measurement of the Noise Resulting from the Interaction of Turbulence with a Lifting Surface," *International Journal of Aeroacoustics*, Vol. 11, 2012, pp. 675-700.

4. Palleja-Cabre, S., Chaitanya, P., Joseph, P., Kim, J.W., Priddin, M.J., Ayton, L.J., Geyer, T.F., and Chong, T.P., "Downstream Porosity for the Reduction

of Turbulence-Aerofoil Interaction Noise." *Journal of Sound and Vibration*, Vol. 541, December 2022, 117324.

5. Bowen, L., Celik, A., and Azarpeyvand, M., "A Thorough Experimental Investigation on Airfoil Turbulence Interaction Noise," *Physics of Fluids*, Vol. 35, March 2023.

6. Nark, D.M. and Jones, M.G., "A Fundamental Study of Bifurcation Acoustic Treatment Effects on Aft-Fan Engine Noise," AIAA Paper 2023-3345, June 2023.

7. Merino-Martinez, R., Carpio, A.R., Pereira, L.P.L., van Herk, S., Avallone, F., Ragni, D., and Kotsonis, M., "Aeroacoustic Design and Characterization of the 3D-Printed, Open-Jet, Anechoic Wind Tunnel of Delft University of Technology," *Applied Acoustics*, Vol. 170, December 2020, 107504.

8. Pascioni, K., Reger, R., Edstrand, A., and Cattafesta, L., "Characterization of an Aeroacoustic Wind Tunnel Facility," 43rd International Congress and Exposition of Noise Control Engineering, November 2014.

9. Bahr, C.J., "Toward Relating Open- and Closed-Test Section Microphone Phased Array Aeroacoustic Measurements," AIAA Paper 2021-2127, August 2021.

10. Devenport, W.J., Burdisso, R.A., Borgoltz, A., Ravetta, P.A., Barone, M.F., Brown, K.A., and Morton, M.A., "The Kevlar-Walled Anechoic Wind Tunnel," *Journal of Sound and Vibration*, Vol. 332, August 2013, pp. 3971-3991.

11. Lighthill, M.J., "On Sound Generated Aerodynamically," *Proceedings of the Royal Society A*, Vol. 211, March 1952, pp. 564-587.

12. Schlicting, H., *Boundary Layer Theory*, McGraw-Hill, 1979.

13. NWTC Government/Industry Team, "National Wind Tunnel Complex (NWTC) Final Report," NASA CR-198491, June 1996.

14. King, R.A., Andino, M.Y., Melton, L., Eppink, J., and Kegerise, M.A., "Flow Disturbance Measurements in the National Transonic Facility," *AIAA Journal*, Vol. 52, January 2014, pp. 116-130.

15. White, F.M., *Viscous Fluid Flow*, McGraw-Hill, 2006.